SCIENTIFIC REPORTS

OPEN

A multiscale computational model predicts distribution of anti-angiogenic isoform VEGF$_{165b}$ in peripheral arterial disease in human and mouse

Liang-Hui Chu[1], Vijay Chaitanya Ganta[2], Min H. Choi[2], George Chen[1], Stacey D. Finley[3], Brian H. Annex[2] & Aleksander S. Popel[1]

Angiogenesis is the growth of new blood vessels from pre-existing microvessels. Peripheral arterial disease (PAD) is caused by atherosclerosis that results in ischemia mostly in the lower extremities. Clinical trials including VEGF-A administration for therapeutic angiogenesis have not been successful. The existence of anti-angiogenic isoform (VEGF$_{165b}$) in PAD muscle tissues is a potential cause for the failure of therapeutic angiogenesis. Experimental measurements show that in PAD human muscle biopsies the VEGF$_{165b}$ isoform is at least as abundant if not greater than the VEGF$_{165a}$ isoform. We constructed three-compartment models describing VEGF isoforms and receptors, in human and mouse, to make predictions on the secretion rate of VEGF$_{165b}$ and the distribution of various isoforms throughout the body based on the experimental data. The computational results are consistent with the data showing that in PAD calf muscles secrete mostly VEGF$_{165b}$ over total VEGF. In the PAD calf compartment of human and mouse models, most VEGF$_{165a}$ and VEGF$_{165b}$ are bound to the extracellular matrix. VEGF receptors VEGFR1, VEGFR2 and Neuropilin-1 (NRP1) are mostly in 'Free State'. This study provides a computational model of VEGF$_{165b}$ in PAD supported by experimental measurements of VEGF$_{165b}$ in human and mouse, which gives insight of VEGF$_{165b}$ in therapeutic angiogenesis and VEGF distribution in human and mouse PAD model.

Angiogenesis is the process of new blood vessel formation from the pre-existing microvessels. Members of vascular endothelial growth factor (VEGF) superfamily critically but differentially regulate angiogenesis in normal physiological and pathophysiological conditions including exercise, ischemic cardiovascular diseases, and cancer[1]. The VEGF family includes five ligands VEGF-A, VEGF-B, VEGF-C, VEGF-D and PlGF (Placental growth factor), and five receptors VEGFR1, VEGFR2, VEGFR3, NRP1 (neuropilin-1) and NRP2 (neuropilin-2). Among the members of VEGF family, VEGF-A and VEGFR2 are considered to be potent pro-angiogenic molecules. However, recent identification of VEGF$_{xxxb}$ isoforms has changed the classical paradigm of VEGF-A:VEGFR2 function in regulation of angiogenesis[2].

Alternate splicing in the 8th exon of VEGF-A results in the formation of sister families: pro-angiogenic VEGF$_{xxxa}$ (VEGF$_{165a}$, in human) isoform (xxx denotes number of amino acids) containing an amino acid sequence 'CDKPRR' and anti-angiogenic VEGF$_{165b}$ isoform containing an amino acid sequence 'PLTGKD' in their C-terminus, respectively. The positively charged cysteine and arginine residues (CDKPRR) in pro-angiogenic VEGF-A isoform facilitate the binding of VEGF$_{165a}$ to VEGFR2 and NRP1 to induce a conformational change and internal rotation of intracellular domain and maximal activation of VEGFR. However, replacement of cysteine and arginine residues with neutral lysine and aspartic acid in VEGF$_{xxxb}$ isoform was predicted to result in partial

[1]Department of Biomedical Engineering, School of Medicine, Johns Hopkins University, Baltimore, MD 21205, United States. [2]Cardiovascular Medicine, Department of Medicine, and the Robert M. Berne Cardiovascular Research Center University of Virginia School of Medicine, Charlottesville, VA 22901, United States. [3]Department of Biomedical Engineering, University of Southern California, Los Angeles, California 90089, United States. Correspondence and requests for materials should be addressed to A.S.P. (email: apopel@jhu.edu)
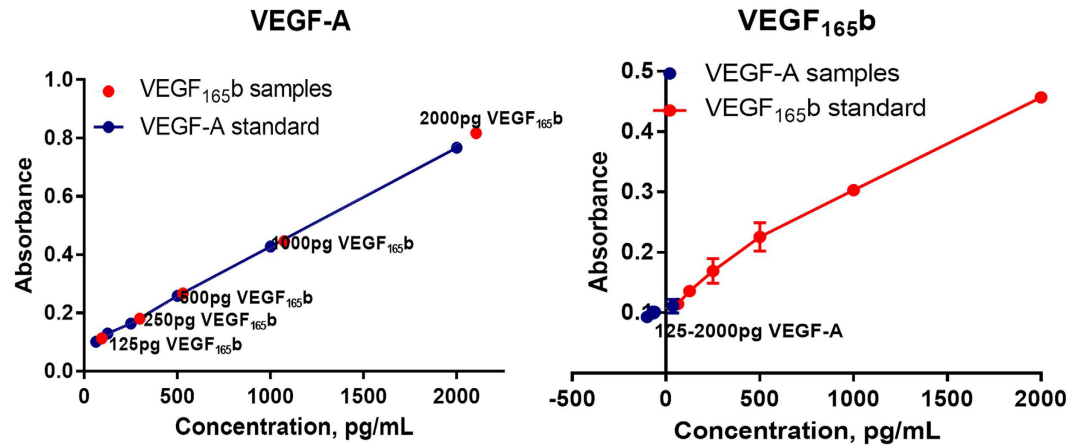
    1

Figure 1. ELISA showing the specificity and sensitivity of VEGF$_{165a}$ (VEGFA) and VEGF$_{165b}$ antibodies.
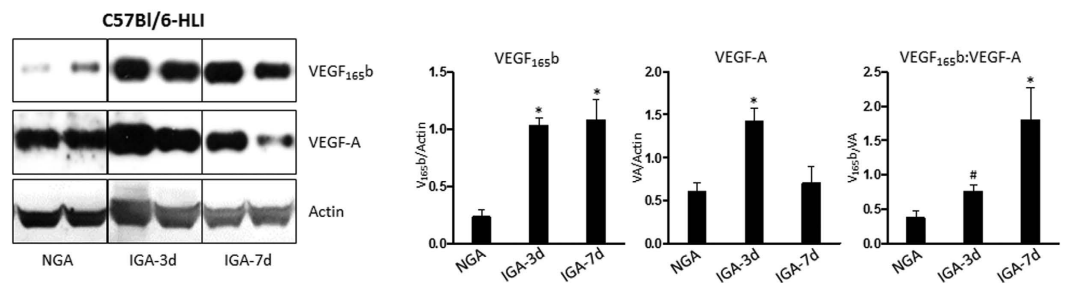

Figure 2. Western blot analysis of VEGF$_{165b}$, VEGF-A and Actin in non-ischemic (NGA) and ischemic gastrocnemius muscle (IGA) at day 3 and day 7 post hindlimb ischemia (HLI). (n = 4. One-way ANOVA with Dunnetts post-test. p < 0.05 considered significant).

VEGFR2 activation that cannot induce torsional rotation required for autophosphorylation and downstream signaling. Hence, the balance between VEGF$_{165a}$ and VEGF$_{165b}$ levels may play a crucial role in promoting angiogenesis especially in ischemic cardiovascular diseases such as peripheral arterial disease (PAD) or coronary artery disease (CAD).

PAD is caused by atherosclerosis, which results in ischemia most frequently in the lower extremities. Clinical trials including exogenous VEGF-A administration to activate VEGFR2 dependent therapeutic angiogenesis were not successful. While suboptimal delivery or dosage might be the contributing factors, induction of VEGF$_{165b}$ in ischemic muscle could compete with pro-angiogenic VEGF$_{165a}$ isoform for binding sites on VEGFR2 to decrease VEGFR2 activation. The mechanism of VEGF$_{165b}$ binding to VEGFR2 suggests the potential reason for the failure of therapeutic angiogenesis in VEGF-A clinical trials. Currently, the balance between VEGF$_{165b}$ and VEGF$_{165a}$ isoforms that can modulate VEGFR2 activation and angiogenic signaling in the ischemic skeletal muscle of PAD patients is not fully understood.

We have previously reported experimental evidence that VEGF$_{165b}$ levels are significantly higher in biopsies of PAD patients[3]. Kikuchi *et al.* measured the ratios of VEGF$_{165b}$ versus VEGF$_{165a}$ in serum (by western blot analysis) and peripheral blood mononuclear cells (PBMCs, by mRNA) in PAD patients, which are 4:1 and 8:1, respectively[4]. Currently there is no study measuring the ratio of VEGF$_{165b}$ and VEGF$_{165a}$ in the calf muscles to correlate with VEGFR2 activation in PAD patients. Besides, the understanding of the secretion rates of VEGF$_{165b}$ in different compartments such as diseased calf muscles, blood and normal tissues (all tissues and organs except the diseased calf) is currently lacking. In this study, we expand the previously developed three-compartment models[5,6] to predict the concentration of VEGF$_{165b}$ and VEGF$_{165a}$ in PAD patients. We also report the experimental measurements of the expression level of VEGF$_{165b}$ and VEGF$_{164a}$ in experimental PAD non-ischemic and ischemic muscle samples in mice with hindlimb ischemia to support our computational models.

Results

In this study, we use both experimental and computational approaches to predict the secretion rate of VEGF$_{165b}$ and receptor occupancy of VEGFR1 and VEGFR2 in PAD. In practice, it is not possible to measure the secretion rates of VEGF in different tissues *in vivo*. These important physiological parameters could be only estimated or calculated from the model. This is the first computational model to investigate and account for the experimental ratios of VEGF$_{165b}$ and total VEGF$_{165}$ in human PAD muscle biopsies. The predominance of VEGF$_{165b}$ in human muscles provides the potential mechanism why the clinical trials of VEGF therapeutic angiogenesis
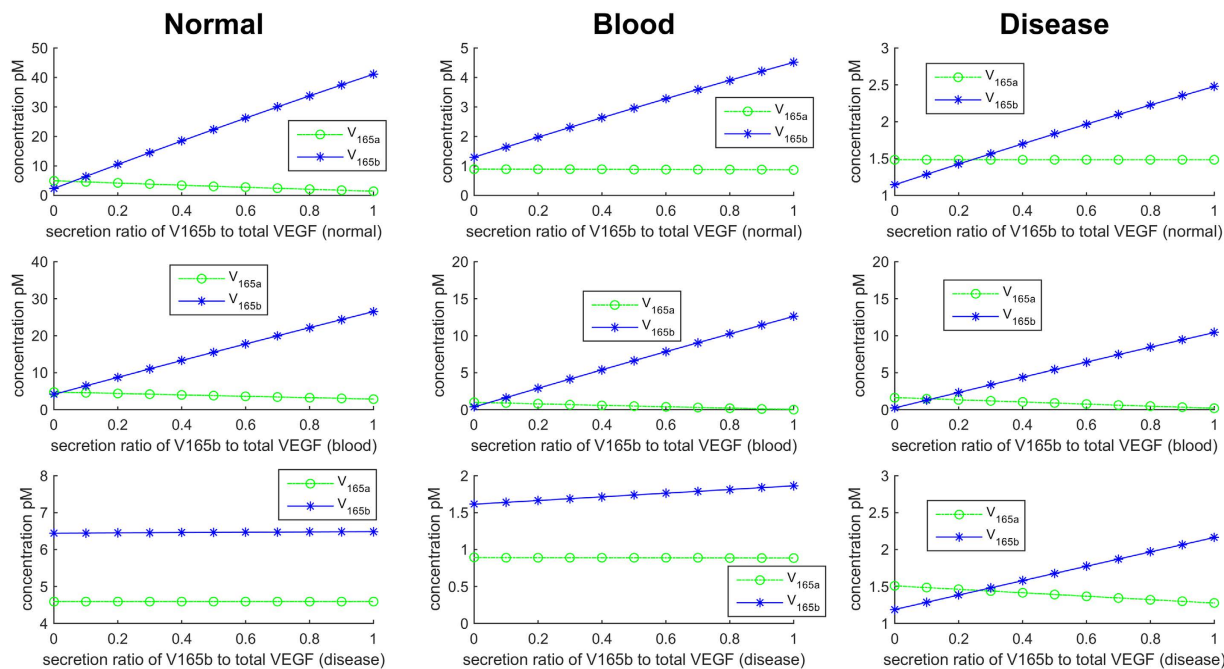
Figure 3. Concentrations of VEGF$_{165a}$ and VEGF$_{165b}$ plotted against the secretion ratio of VEGF$_{165b}$ to total VEGF$_{165}$ isoforms in normal (left column), blood (middle column) and disease compartments (right column). Each row represents the variation of secretion ratio of VEGF$_{165b}$ to total VEGF$_{165}$ in (**A**) normal, (**B**) blood, and (**C**) disease compartment.
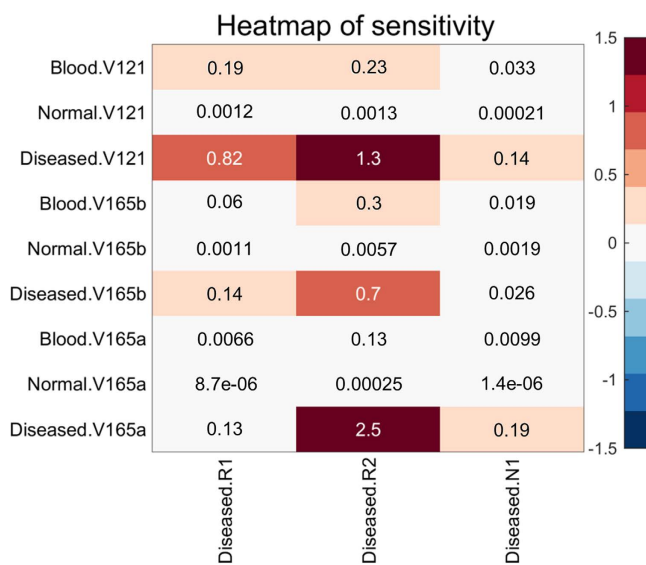

Figure 4. Local sensitivity analysis for VEGF$_{165a}$, VEGF$_{165b}$ and VEGF$_{121}$. The results show that VEGF$_{165a}$ in the disease compartment and VEGF$_{165b}$ in the blood compartment are more sensitive to VEGFR2 than VEGFR1, whereas VEGF$_{121}$ in the disease and blood compartment is sensitive to both VEGFR1 and VEGFR2. VEGF$_{165a}$, VEGF$_{165b}$, VEGF$_{121}$ are not sensitive to NRP1. The sensitivity analysis demonstrates the importance of VEGF$_{165b}$-VEGFR2 binding.

have failed. Based on the measurement of ratio of VEGF$_{165b}$ and total VEGF$_{165}$ in muscle biopsies, we use the three-compartment model to predict the secretion rates of VEGF$_{165b}$ in different tissues. This model enables prediction of receptor occupancy with VEGF$_{165b}$ and other isoforms in human and mouse.

Specificity and sensitivity of VEGF-A and VEGF$_{165b}$ antibodies. VEGF-A ELISA detected both recombinant VEGF$_{165a}$ and VEGF$_{165b}$ with equal sensitivity and specificity. This result indicates that the actual
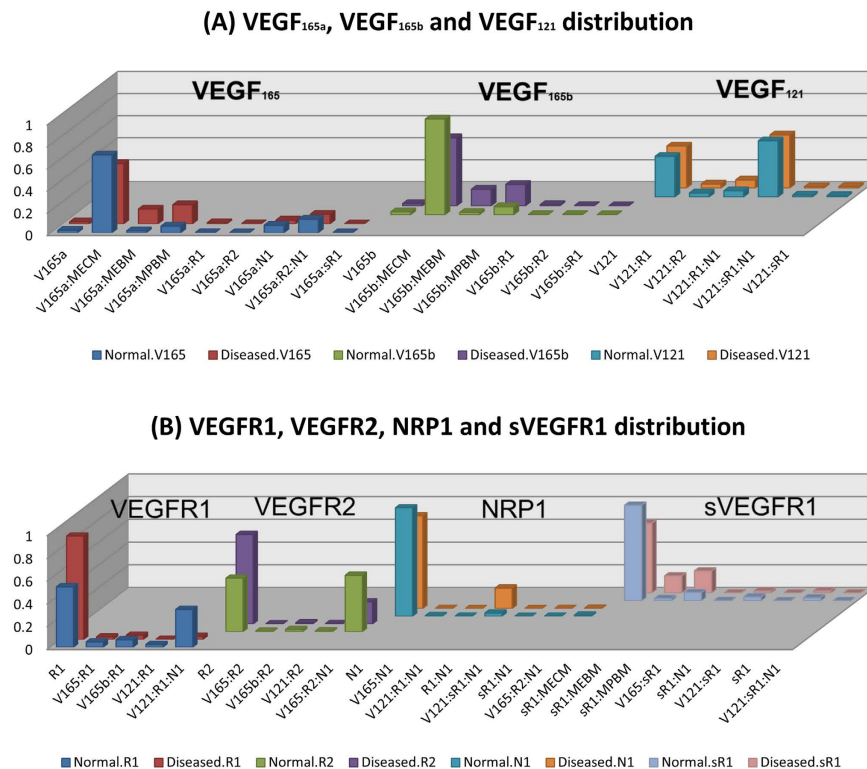
(A) VEGF$_{165a}$, VEGF$_{165b}$ and VEGF$_{121}$ distribution

(B) VEGFR1, VEGFR2, NRP1 and sVEGFR1 distribution

Figure 5. (**A**) VEGF distribution and (**B**) VEGFR occupancy in human. The bars in y-axis represent the percentage of each species for each VEGF ligand VEGF$_{165a}$, VEGF$_{165b}$ and VEGF$_{121}$ in (**A**) and each receptor VEGFR1, VEGFR2, NRP1, and sVEGFR1 in (**B**).

measurement of pro-angiogenic VEGF-A by VEGF-A antibodies have been overestimated due to its cross reactivity with anti-angiogenic VEGF$_{165b}$ isoforms. However, VEGF$_{165b}$ antibody raised against the unique 6 amino acid sequence (SLTRKD) used in ELISA specifically detected only recombinant VEGF$_{165b}$ but not recombinant VEGF$_{165a}$ at any concentrations indicating that a ratio of VEGF$_{165b}$:total VEGF$_{165}$ measurements will be needed to determine the actual amount of pro-angiogenic VEGF-A isoforms in biological samples (Fig. 1).

Three-compartmental models of PAD: motivation, assumptions and simulations. In our western analysis we observed a significant increase in total VEGF$_{165}$ levels in ischemic muscle compared to non-ischemic at day 3 and day 7 post hindlimb ischemia (HLI). However, the levels of VEGF$_{165b}$ were also significantly higher at day 3 and day 7 post HLI. The ratio VEGF$_{165b}$:VEGF-A (from the densitometry values of western blot analysis) showed a ~4 fold induction in the fraction of VEGF$_{165b}$ in total VEGF-A in ischemic muscle at day 7 post HLI compared to non-ischemic (i.e. VEGF$_{165b}$ isoforms constitute ~80% of total VEGF-A) in experimental PAD muscle compared to control (Fig. 2).

We used the above experimental results in our model to predict the concentrations of VEGF$_{165b}$ and VEGF$_{165a}$ in the calf muscles. Kikuchi *et al.* measured the ratios of VEGF$_{165b}$ versus VEGF$_{165a}$ in serum (protein) and peripheral blood mononuclear cells (PBMCs, mRNA) in PAD patients, which were reported as 4:1 and 8:1, respectively[4]. Hoier *et al.* measured the interstitial total VEGF protein concentration (i.e. including both VEGF$_{165a}$ and VEGF$_{165b}$) in the thigh skeletal muscle of PAD patients as 69 ± 21 and 190 ± 78 pg/ml in rest and active exercise, respectively. We convert these numbers to molar concentrations as $69 \text{ pg/ml} \cdot 1000 \text{ ml/l} \cdot 1 \text{ mole}/46000 \text{ g} = 1.5 \text{ pM}$ and $190 \text{ pg/ml} = 4.1 \text{ pM}$, respectively, based on the molecular weight 46 kDa for VEGF homodimers[7]. We have constrained the model so that the predictions of steady-state concentration of VEGF$_{165b}$ and total VEGF$_{165}$ are within an experimentally observed range (e.g. 0–10 pM) in any of the three compartments to be consistent with the experimental data.

However, because of the sparseness of experimental data it is not possible to identify all the unknown parameters from the available data. Thus, we choose an initial set of secretion rates based on our previous analyses and perform the sensitivity analysis to determine a range of secretion rates constrained with available experimental data, both our own and others. Note that future experiments may provide additional data that could allow further constraining the solutions; presently, the analysis is heuristic aiming at stimulating further experiments.

Prediction of secretion rates of VEGF$_{165b}$ and secretion ratio of VEGF$_{165b}$ over total VEGF in three compartments. The values of secretion rate of VEGF in normal and blood compartments are adopted from the tumor angiogenesis model[8]. The secretion rate in PAD calf compartment is set up the same as the secretion rate in the normal compartment. The initial set of secretion rates of total VEGF including VEGF$_{165a}$, VEGF$_{165b}$ and VEGF$_{121}$ is assumed as 0.02, 0.031 and 0.02 molecules/cell/s, respectively, in all the three compartments (normal, blood and

(A) VEGF₁₆₄ₐ, VEGF₁₆₄ᵦ and VEGF₁₂₀ distribution

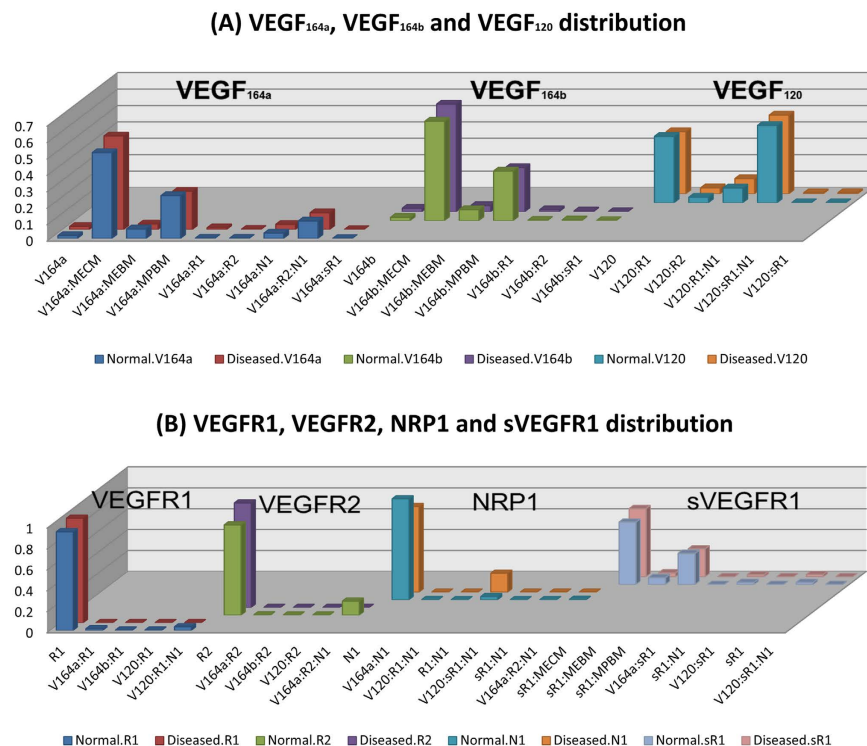### (B) VEGFR1, VEGFR2, NRP1 and sVEGFR1 distribution

Figure 6. (**A**) VEGF distribution and (**B**) VEGFR occupancy in mouse. The bars represent the percentage of each species for each VEGF ligand in (**A**) and each receptor in (**B**), respectively, same as Fig. 5.

Compartments	Diseased PAD calf (Total VEGF secretion rate: 0.02 molecules/cell/s)	Blood (Total VEGF secretion rate: 0.031 molecules/cell/s)	Normal (Total VEGF secretion rate: 0.02 molecules/cell/s)
Species			
VEGF$_{165a}$	1.276 pM	0.886 pM	4.591 pM
VEGF$_{165b}$	2.163 pM	1.863 pM	6.486 pM
VEGF$_{121}$	0.701 pM	0.653 pM	2.416 pM

Table 1. Prediction of VEGF$_{165b}$, VEGF$_{165a}$ and VEGF$_{121}$.

PAD calf). The secretion ratio of VEGF$_{121}$ over total VEGF (VEGF$_{165a}$ + VEGF$_{165b}$ + VEGF$_{121}$) is assumed to be 10%, i.e. 0.002, 0.0031 and 0.002 in normal, blood and disease compartments, respectively. We scan the ratio of secretion rate of VEGF$_{165b}$ over total VEGF$_{165}$ (i.e. the sum of VEGF$_{165a}$ and VEGF$_{165b}$) in the three compartments from 0 and 1 in 0.1 increments. When the ratio of VEGF$_{165b}$ over total VEGF$_{165}$ is 0.5 in all three compartments (i.e. secretion rates of VEGF$_{165a}$ and VEGF$_{165b}$ have equal values 0.009, 0.01395 and 0.009 in normal and disease compartments, respectively), the concentration of VEGF$_{165b}$ in the normal compartment reaches 31 pM. When the ratio of VEGF$_{165b}$ over total VEGF$_{165}$ in all three compartments is 10%, the concentration of VEGF$_{165b}$ in the normal compartment drops to 6.5 pM, which is within the experimentally observed range (<10 pM).

We can also change the secretion ratio of VEGF$_{165b}$ to total VEGF$_{165}$ in each of the three compartments individually. We plot the predictions for steady-state concentrations of VEGF$_{165b}$ and VEGF$_{165a}$ in Fig. 3. We first change the secretion ratio of VEGF$_{165b}$/total VEGF$_{165}$ from 0 to 1 in 0.1 increments in the normal compartment while keeping the total secretion rate of VEGF$_{165}$ (VEGF$_{165a}$ + VEGF$_{165b}$) constant at 0.018 molecules/cell/s in the normal and disease compartments and fixing the secretion ratios in blood and disease compartments at 0.1 (Fig. 3A). We follow the same strategy in Fig. 3B,C, except we vary the secretion ratio of VEGF$_{165b}$/total VEGF$_{165}$ in the blood compartment for B and the disease compartment for C, while the total secretion rates are fixed and the ratios are fixed at 0.1 in the other compartments. The model predicts that the concentration of VEGF$_{165b}$ remains at approximately 6.5 pM, when the VEGF$_{165b}$/total VEGF$_{165}$ secretion ratio is 0.1 in normal and blood, across the full range of secretion ratios in the disease compartment (Fig. 3, left column). Additionally, the steady state concentration of VEGF$_{165b}$ is consistently predicted to be approximately 30% higher than VEGF$_{165a}$ in the disease compartment. This result is qualitatively consistent with our experimental data. This prediction gives us an important biological insight that the PAD disease calf muscles comprise mostly VEGF$_{165b}$ over other total VEGF isoforms. This finding could be further extended for the development of VEGF$_{165b}$ antibody treatment in PAD.

Sensitivity analysis of VEGF₁₆₅ₐ, VEGF₁₆₅ᵦ and sVEGFR1.

We use SimBiology to perform a local sensitivity analysis, which quantifies how changes in a given parameter value influence predicted concentrations of interest.
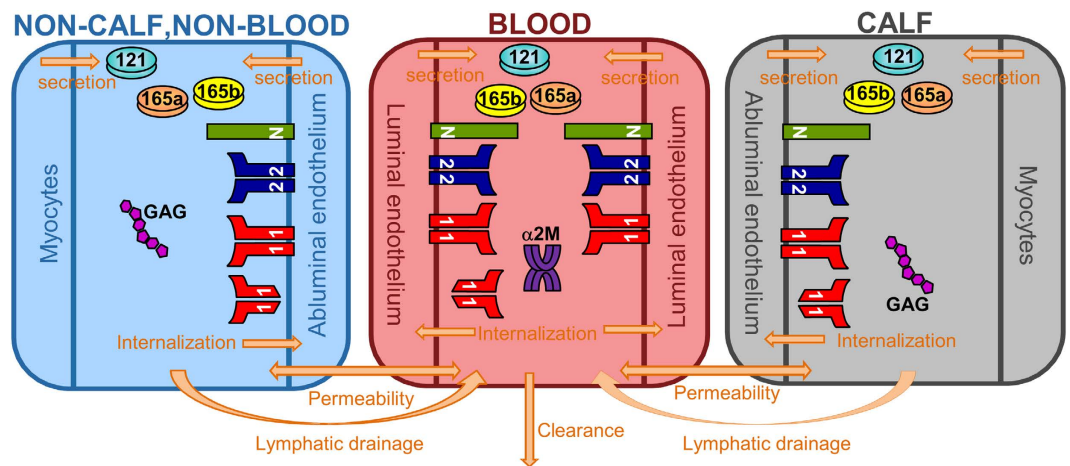
Figure 7. Three-compartment model of VEGF in peripheral arterial disease. 121: $VEGF_{121}$. 165a: $VEGF_{165a}$. 165b: $VEGF_{165b}$. N: neuropilin-1. 1: soluble and membrane-bound VEGFR1. 2: VEGFR2. GAG: glycosaminoglycan. $\alpha 2M$: alpha-2 macroglobulin.

	Value	Units	Resources
Human PAD geometric parameters			
Compartment volume	738	cm³	Combined volume of lateral gastrocnemius, medial gastrocnemius, soleus muscles[20]
Fluid volume in ECM	31.87%	cm³/cm³ tissue	Calculated from ref. 14
Fluid volume in EBM	0.45%	cm³/cm³ tissue	Calculated from ref. 14
Fluid volume in PBM	0.58%	cm³/cm³ tissue	Calculated from ref. 14
Muscle fiber cell surface area	417	cm²/cm³ tissue	Calculated from ref. 14
Muscle fiber cross-sectional area	3,464	μm²	Calculated from refs 21–23
Mouse PAD geometric parameters			
Compartment volume	0.01	cm³	6
Fluid volume in ECM	28.92%	cm³/cm³ tissue	6
Fluid volume in EBM	0.097%	cm³/cm³ tissue	6
Fluid volume in PBM	0.68%	cm³/cm³ tissue	6
Muscle fiber cell surface area	713.68	cm²/cm³ tissue	Based on mouse myocytes[13]
Muscle fiber cross-sectional area	2500	μm²	Based on mouse myocytes[13]

Table 2. Geometric parameters for the PAD calf compartment in human and mouse.

We calculate the normalized sensitivity coefficient $\frac{X}{Y} \cdot \frac{\partial [Y]}{\partial [X]}$ based on the algorithm[9], where Y is the species $VEGF_{165a}$, $VEGF_{165b}$ and $VEGF_{121}$, and X is the three VEGF receptors VEGFR1, VEGFR2 and NRP1 in the disease compartments; [X] and [Y] denote the molar concentrations. Figure 4 shows that $VEGF_{165a}$ in the disease compartment and $VEGF_{165b}$ in the blood compartment are more sensitive to VEGFR2 than VEGFR1, whereas $VEGF_{121}$ in the disease and blood compartment is sensitive to both VEGFR1 and VEGFR2. $VEGF_{165a}$, $VEGF_{165b}$, $VEGF_{121}$ are not sensitive to NRP1. The sensitivity analysis in Fig. 4 demonstrates the importance of $VEGF_{165b}$-VEGFR2 binding.

Tissue VEGF distribution and VEGFR occupancy in human three compartment model. We show the steady-state distribution of VEGF ligands and their receptors for each tissue in Fig. 5A,B, respectively. The y-axis represents the percentage of each species in x-axis in each VEGF ligand ($VEGF_{165a}$, $VEGF_{165b}$ and $VEGF_{121}$) in Fig. 5A and each receptor (VEGFR1, VEGFR2, NRP1, and sVEGFR1) in Fig. 5B. In PAD calf, most $VEGF_{165a}$ is bound to the ECM and parenchymal basement membrane (PBM) (55% and 17%, respectively); most $VEGF_{165b}$ is also bound to ECM and PBM (62% and 20%, respectively). Here ECM represents the total extracellular matrix minus the endothelial and parenchymal basement membranes. Most $VEGF_{121}$ isoform is bound to VEGFR1 and NRP1 as the $VEGF_{121}$:VEGFR1:NRP1 complex in the disease (48%) and normal (51%) compartment. Regarding receptor occupancy, in the normal compartment, the three receptors VEGFR1, VEGFR2 and NRP1 are in the free states, except the $VEGF_{121}$:VEGFR1:NRP1 (33%) and $VEGF_{165a}$:VEGFR2:NRP1 (49%). In the PAD calf compartment, most receptors are in the free states, except the complexes $VEGF_{165a}$:VEGFR2:NRP1 (20%) and VEGFR1:NRP1 (18%). Most sVEGFR1 are bound to ECM, endothelial basement membrane (EBM) and PBM (62%, 15% and 19%, respectively). Our model in PAD resembles the similar distribution of VEGF and VEGFR occupancy in tumor[10].
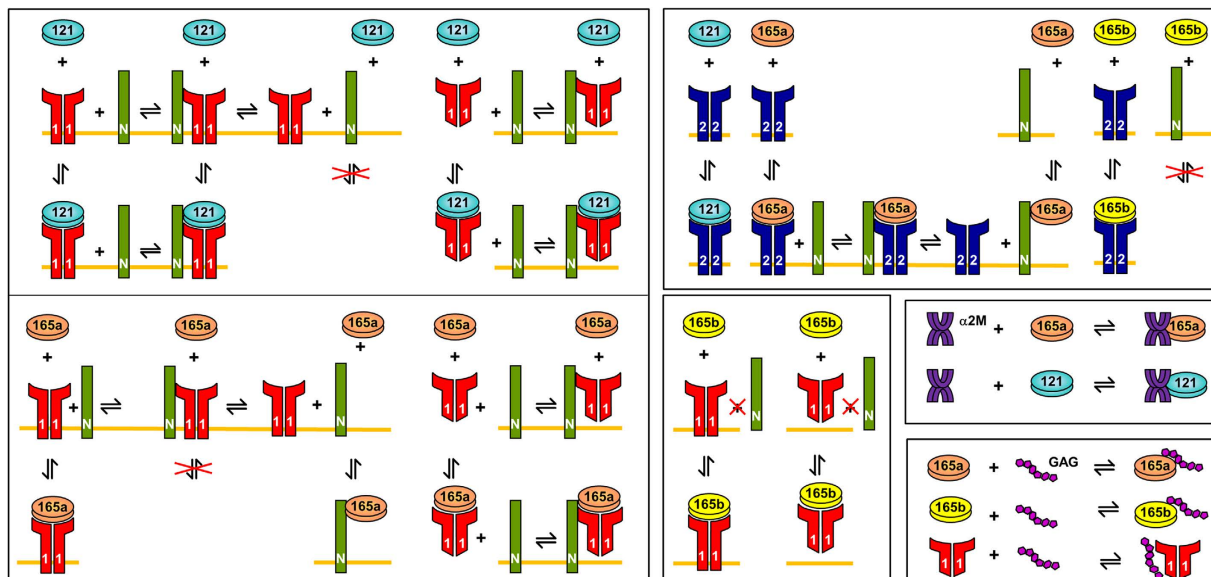
Figure 8. Molecular Interactions of VEGF$_{165a}$, VEGF$_{165b}$ and VEGF$_{121}$.

Receptors	Value	Units	References
R1: Abluminal EC (normal)	3,750	receptors/EC	24,25
R2: Abluminal EC (normal)	300	receptors/EC	24,25
N1: Abluminal EC (normal)	20,000	receptors/EC	Extrapolated from receptor density on normal ECs, accounting for different cell surface areas
R1: Abluminal EC (Disease)	0	receptors/EC	24
R2: Abluminal EC (Disease)	0	receptors/EC	24
N1: Abluminal EC (Disease)	34,500	receptors/EC	24

Table 3. Number of cell surface receptors VEGFR1, VEGFR2 and NRP1. Units of values: dimers/EC in VEGFR1 and VEGFR2 and dimer/EC in NRP1; EC: endothelial cell.

VEGF distribution and VEGFR occupancy in murine three compartment model. Constructing a computational model of mouse VEGF distribution is necessary to make use of the experimental measurements in hindlimb ischemia (HLI) models in mice where numerous studies have been conducted[3,11,12]. In the mouse, VEGF isoforms are shorter by one amino acid, e.g., VEGF$_{164a}$, and VEGF$_{120}$, but VEGF$_{165b}$. Construction of the three-compartment model in mouse can help identify the relative concentration of VEGF$_{164a}$ and VEGF$_{165b}$ in the different compartments, and predict VEGF receptor occupancy. We replace the geometric parameters in the three-compartment model from human to mouse. These geometric parameters of mouse are described in the tumor xenograft model[6] as well as in the mouse two-compartment model[13]. The results of VEGF distribution and VEGFR occupancy are shown in Fig. 6(A,B), respectively. Figures 5(A) and 6(A) show that VEGF$_{165b}$ (human and mouse) mostly bind to the ECM and rarely exist as free ligands in both human and mouse. VEGF$_{164a}$ and VEGF$_{165b}$ bind to PBM with higher percentage in mouse than the corresponding isoforms in human. The VEGF receptor occupancies in Figs 5(B) and 6(B) show the similar trend between mouse and human. However, there is lower percentage of free VEGFR1 and VEGFR2 in human (Fig. 5B) than in mouse (Fig. 6B). This result is due to the higher percentage of VEGF$_{121}$:VEGFR1:NRP1 and VEGF$_{165a}$:VEGFR2:NRP1 in human than the corresponding complexes in mouse.

Discussion

We previously developed the three-compartment models of VEGF in tumor[6,8,10] and in PAD[14]. The anti-angiogenic form of VEGF$_{165b}$ has not been included in any of the previous computational models; this is the first study to include VEGF$_{165b}$ in our human PAD model. This is also the first study that compares human PAD and mouse hindlimb ischemia (HLI) models. By changing the geometric parameters in human PAD calf muscles and adding the kinetics equations of VEGF$_{165b}$, we predict the VEGF$_{165b}$ level in the PAD calf, blood and normal tissue compartments. We summarize the predictions in Table 1. Our computational model shows that the ratio of VEGF$_{165b}$/VEGF$_{165a}$ in PAD is higher than 1 (1.70, 2.10 and 1.41 in disease, blood and normal compartments, respectively). This prediction is consistent with the experimental measurements of VEGF$_{165b}$ as the predominant isoform of VEGF in PAD[4]. The ratio of VEGF$_{165b}$/total VEGF$_{165}$ in the disease compartment of our model is

	Value	unit	References
VEGF$_{165a}$, VEGF$_{165b}$ and VEGF$_{121}$ binding to VEGFR1			
k_{on}	3×10^7	$M^{-1}s^{-1}$	26,27
k_{off}	10^{-3}	s^{-1}	26,27
K_d	33	pM	26,27
VEGF$_{165a}$, VEGF$_{165b}$ and VEGF$_{121}$ binding to VEGFR2			
k_{on}	10^7	$M^{-1}s^{-1}$	26,27
k_{off}	10^{-3}	s^{-1}	26,27
K_d	100	pM	26,27
VEGF$_{165a}$ and VEGF$_{121}$ binding to NRP1			
k_{on}	3.2×10^6	$M^{-1}s^{-1}$	26,27
k_{off}	10^{-3}	s^{-1}	26,27
K_d	312.5	pM	26,27
VEGF$_{165a}$, VEGF$_{165b}$ and VEGF$_{121}$ binding to GAGs			
k_{on}	4×10^5	$M^{-1}s^{-1}$	26,27
k_{off}	10^{-2}	s^{-1}	26,27
K_d	23.8	pM	26,27
VEGF$_{165a}$, VEGF$_{165b}$ and VEGF$_{121}$ binding to α2M			
k_{on}	25	$M^{-1}s^{-1}$	Calculated
k_{off}	10^{-4}	s^{-1}	Assumed
K_d	4.0	μM	28
VEGF$_{165a}$, VEGF$_{165b}$ and VEGF$_{121}$ binding to α2M$_{fast}$			
k_{on}	2.4×10^2	$M^{-1}s^{-1}$	Calculated
k_{off}	10^{-4}	s^{-1}	Assumed
K_d	0.42	μM	28
VEGF$_{165a}$, VEGF$_{165b}$ and VEGF$_{121}$ binding to sVEGFR1			
k_{on}	3×10^7	$M^{-1}s^{-1}$	Assume, based on VEGF binding to VEGFR1
k_{off}	10^{-3}	s^{-1}	Assumed
K_d	33	pM	Assumed
Coupling of NRP1 and VEGFR1			
k_c	10^{14}	$(Mol/cm^2)^{-1}s^{-1}$	26,27
k_{off}	10^{-2}	s^{-1}	26,27
Coupling of NRP1 and VEGFR2			
$k_{c\,V165R2,N1}$	3.1×10^{13}	$(Mol/cm^2)^{-1}s^{-1}$	26,27
$k_{off\,V165R2,N1}$	10^{-3}	s^{-1}	26,27
$k_{c\,V165N1,R2}$	10^{14}	$(Mol/cm^2)^{-1}s^{-1}$	26,27
$k_{off\,V165N1,R2}$	10^{-3}	s^{-1}	26,27
sVEGFR1 binding to NRP1			
k_{on}	5.6×10^6	$M^{-1}s^{-1}$	Calculated
k_{off}	10^{-2}	s^{-1}	Assumed, based on VEGFR1 coupling to NRP1
K_d	1.8	nM	29
sVEGFR1 binding to GAGs			
k_{on}	4.2×10^5	$M^{-1}s^{-1}$	Assumed, based on VEGF binding to GAG
k_{off}	10^{-2}	s^{-1}	Assumed
K_d	24	pM	Assumed

Table 4. Kinetic parameters.

slightly lower than the experiment in human biopsies; however, it should be noted that our predictions are for VEGF concentration in the interstitial fluid in the normal and diseased tissues, whereas the measurements represent the bulk tissue including intracellular components.

We do not include intrinsic heterogeneity that arises from the stochastic nature of biochemical reactions because we consider relatively large concentrations (pM). It may be more relevant to consider extrinsic heterogeneity (i.e., due to variations in protein concentrations)[15]. Others have included heterogeneity in the receptor distributions[16] and found that variability in receptor expression can influence the response to anti-VEGF cancer treatment. The focus of the present work is to investigate and quantify how VEGF$_{165b}$ molecular interactions influence overall VEGF distribution in human and mouse. This is the first model to incorporate the VEGF$_{165b}$ isoform

	Value	unit	References
Permeability between normal and blood compartments			
VEGF	4.0×10^{-8}	cm/s	27
sVEGFR1	1.5×10^{-8}	cm/s	30
VEGF:sVEGFR1 complex	1.5×10^{-8}	cm/s	30
Permeability between disease and blood compartments			
VEGF	4.0×10^{-7}	cm/s	Assumed, based on high permeability in PAD
sVEGFR1	3.0×10^{-7}	cm/s	Assumed
VEGF:sVEGFR1 complex	1.5×10^{-7}	cm/s	Assumed
Clearance			
VEGF	1.1×10^{-3}	s^{-1}	Calculated, based on half-life
sVEGFR1	5.0×10^{-6}	s^{-1}	30
VEGF:sVEGFR1	3.0×10^{-4}	s^{-1}	30
α2M	3.9×10^{-5}	s^{-1}	31
VEGF:α2M complex	3.9×10^{-5}	s^{-1}	Assumed, based on α2M
α2M$_{fast}$	3.9×10^{-3}	s^{-1}	32
VEGF:α2M$_{fast}$ complex	3.9×10^{-3}	s^{-1}	Assumed, based on α2M$_{fast}$
Degradation			
sVEGFR1	1.9×10^{-4}	s^{-1}	Assumed, based on VEGF
VEGF:sVEGFR1 complex	1.9×10^{-4}	s^{-1}	Assumed, based on VEGF
Synthesis			
α2M	3.5×10^{10}	Molecules/cm³ tissue/s	Calculated
α2M$_{fast}$	1.9×10^{10}	Molecules/cm³ tissue/s	Calculated

Table 5. Transport parameters.

and we focus on the issues related to the expression of this isoform. Future work can incorporate variability in protein levels.

This study is also important for computational modeling of pharmacokinetics and pharmacodynamics (PK/PD) of administering VEGF$_{165b}$-antibody as a potential pro-angiogenic therapeutic. Current VEGF antibodies including bevacizumab bind both total VEGF (VEGF$_{165a}$, VEGF$_{165b}$ and VEGF$_{121}$). We propose to introduce an antibody to VEGF$_{165b}$ as a PAD therapeutic to stimulate angiogenesis. This strategy will be explored in upcoming computational and experimental studies.

Conclusions

We applied the three-compartment model of VEGF distribution to predict the concentration of VEGF isoforms, including VEGF$_{165b}$, in the body in peripheral arterial disease. The experimental data show that the expression level of VEGF$_{165b}$ is higher than VEGF$_{165a}$ in the human biopsies and the computational model results are consistent with these measurements. The secretion ratio of VEGF$_{165b}$ to total VEGF$_{165}$ is estimated as 1 in the disease compartment, and 0.1 in the blood and normal compartments. Our predictions support the importance of the VEGF$_{165b}$ in PAD, and provide a foundation for therapeutic inhibition of VEGF$_{165b}$ in PAD in the future. This multiscale model can also provide a basis for simulating the pharmacokinetics of VEGF$_{165b}$ antibody in PAD in human and mouse models.

Methods

ELISA to measure VEGF$_{165b}$ antibody sensitivity. VEGF-A and VEGF$_{165b}$ (R&D) Dual sandwich ELISAs were used to determine the sensitivity and specificity of VEGF-A and VEGF$_{165b}$ antibodies in differentiating recombinant pro-angiogenic VEGF-A (VEGF$_{165a}$) and anti-angiogenic VEGF-A (VEGF$_{165b}$) isoforms. Recombinant VEGF$_{165a}$ and VEGF$_{165b}$ isoforms were serially diluted at 1000, 500, 250, 125 pg/ml concentrations and standard VEGF-A and VEGF$_{165b}$ ELISA were performed according to manufacturer instructions on all the samples to determine the sensitivity and specificity of VEGF-A and VEGF$_{165b}$ Mice.

Murine Model of Hindlimb Ischemia. Hindlimb ischemia (HLI) induced by femoral artery ligation and resection was used as an experimental model of human PAD. All animal experiments were approved by the University of Virginia Animal Care and Use Committee and conformed to the Guide for the Care and Use of Laboratory Animals published by the US National Institutes of Health. HLI was performed on 8- to 12-week-old age and sex matched C57Bl/6 mice as described previously[11,12]. Briefly, mice were anesthetized by a combination of ketamine and Xylazine (ketamine 90 mg/kg and xylazine 10 mg/kg) and femoral artery was ligated and resected from just above the inguinal ligament to its bifurcation at the origin of saphenous and popliteal arteries. The inferior epigastric, lateral circumflex, and superficial epigastric artery branches were also ligated.

Antibodies.   VEGF$_{165b}$ antibody was purchased from Millipore (Clone 56/1, Cat No: MABC595), VEGF-A antibody was purchased from Santa Cruz Biotech (Cat No: SC-7269) and β-Actin was purchased from Sigma (Cat No: A2103).

Western blotting, Densitometry and Statistics.   Mice were sacrificed with an overdose of anesthesia and non-ischemic and ischemic gastrocnemius muscle samples were collected at day 3 and day 7 post HLI. Tissue was homogenized in RIPA with protease inhibitor cocktail. Equal amounts of protein were resolved by Sodium Dodecyl Sulphate-Poly Acrylamide Gel Electrophoresis, transferred onto nitro cell cellulose membranes and western blotted against VEGF$_{165b}$, VEGF-A and Actin by chemiluminescent method. Bands on the film were scanned and quantified by densitometric analysis of the band intensity by NIH image-J (1.6) software. Densitometric values were plotted on Graph PAD Prism 6 or 7 and analyzed for statistical significance. One-way ANOVA with Dunnetts post–test was used to check statistical significance. $p < 0.05$ considered statistically significant.

Three-compartment models for human and mouse.   The model is comprised of three components: normal tissue (representing all tissues and organs except the diseased calf and blood), blood, and diseased calf of PAD (Fig. 7). For clarity, we use the notation VEGF$_{165a}$ to denote the pro-angiogenic isoform; we refer to the combination of VEGF$_{165a}$ and VEGF$_{165b}$ as total VEGF$_{165}$. VEGF$_{165a}$, VEGF$_{165b}$ and VEGF$_{121}$ are secreted by myocytes and possibly stromal cells in the normal tissues and by calf muscles in PAD, respectively, and also by endothelial cells in all compartments. VEGF receptors (VEGFR1 and VEGFR2) and co-receptor neuropilin-1 (NRP1) are localized on the surfaces of endothelial and parenchymal cells. We include soluble VEGFR1 and glycosaminoglycan (GAG) chains in the interstitial space of normal and calf compartments, and alpha-2-macroglobulin (α2M) in the blood. These soluble factors bind VEGF and can be present in high concentrations; therefore, it is important to include them in the model. Geometric parameters are used to characterize the compartment and enable conversion of the concentrations from units used in the model (moles/cm³ tissue) to more standard units (molarity). The geometric parameters in the normal and blood human compartments are described in ref. 17 where applications to cancer are considered. The geometric parameters in the diseased calf compartment are described in ref. 14. The geometric parameters for mouse compartments are described in refs 6 and 13. We list the details of geometric parameters used in our model in Table 2.

Binding of VEGF$_{165a}$, VEGF$_{165b}$ and VEGF$_{121}$ to VEGFR1 and VEGFR2.   The molecular interactions between VEGF isoforms and their receptors are illustrated in Fig. 8. VEGFR1 and VEGFR2 are the transmembrane receptors that bind to VEGF$_{165a}$, VEGF$_{165b}$ and VEGF$_{121}$. VEGF$_{165b}$ has the equivalent binding to VEGFR2 as VEGF$_{165a}$[18], and functions as a competitive inhibitor of the major downstream effects of VEGF$_{165a}$. VEGF$_{165a}$ and VEGF$_{165b}$ are the two glycoproteins with heparin binding domain that can bind the extracellular matrix. VEGF$_{121}$ is a freely diffusible protein lacking a heparin-binding domain. VEGF$_{165b}$ could bind to VEGFR1 and VEGFR2 but cannot bind the co-receptor NRP1 because it lacks exon 8a[19]. The densities of cell receptors VEGFR1, VEGFR2 and NRP1 are listed in Table 3 based on available *in vivo* and *in vitro* experimental data. The kinetic parameters are listed in Table 4. The model is described in terms of 80 ordinary differential equations (ODE) and is presented in the Supplementary File.

We assume that the total secretion rate of VEGF isoforms to be 0.02 molecules/cells/s in the disease and normal compartment, and 0.031 in the blood compartment (see Results for the details). The model equations were implemented in MATLAB R2014b (MathWorks, Natick, MA) using the SimBiology toolbox and were solved with the Sundials solver.

Transport parameters.   Molecular species are transported between compartments via microvascular permeability (k_p) and lymphatic drainage (k_L) as shown in Fig. 7. All isoforms of unbound VEGF and soluble VEGFR1 (sVEGFR1) in the tissue compartments are subject to proteolytic degradation (k_{deg}) and are removed from the blood via plasma clearance (c_v). We list the transport parameters in Table 5.

Sensitivity analysis.   The sensitivity analysis is implemented using Matlab SimBiology toolbox. The time-dependent sensitivities of the species states are calculated with respect to species initial conditions and parameter values in the model. The sensitivity is calculated using $\frac{X}{Y} \cdot \frac{\partial [Y]}{\partial [X]}$, which determines how changes in parameter X influences the output Y by taking the partial derivatives.

References

1. Mac Gabhann, F. & Popel, A. S. Systems biology of vascular endothelial growth factors. *Microcirculation* **15,** 715–738 (2008).
2. Woolard, J., Bevan, H. S., Harper, S. J. & Bates, D. O. Molecular diversity of VEGF-A as a regulator of its biological activity. *Microcirculation* **16,** 572–592 (2009).
3. Jones, W. S. *et al.* Alteration in angiogenic and anti-angiogenic forms of vascular endothelial growth factor-A in skeletal muscle of patients with intermittent claudication following exercise training. *Vasc Med* **17,** 94–100 (2012).
4. Kikuchi, R. *et al.* An antiangiogenic isoform of VEGF-A contributes to impaired vascularization in peripheral artery disease. *Nat Med* **20,** 1464–1471 (2014).
5. Finley, S. D., Angelikopoulos, P., Koumoutsakos, P. & Popel, A. S. Pharmacokinetics of Anti-VEGF Agent Aflibercept in Cancer Predicted by Data-Driven, Molecular-Detailed Model. *CPT Pharmacometrics Syst Pharmacol* **4,** 641–649 (2015).
6. Finley, S. D., Dhar, M. & Popel, A. S. Compartment model predicts VEGF secretion and investigates the effects of VEGF trap in tumor-bearing mice. *Frontiers in oncology* **3,** 196 (2013).
7. Hoier, B. *et al.* Angiogenic response to passive movement and active exercise in individuals with peripheral arterial disease. *J Appl Physiol* (*1985*) **115,** 1777–1787 (2013).
8. Finley, S. D. & Popel, A. S. Effect of tumor microenvironment on tumor VEGF during anti-VEGF treatment: systems biology predictions. *J Natl Cancer Inst* **105,** 802–811 (2013).

9. Ingalls, B. P. & Sauro, H. M. Sensitivity analysis of stoichiometric networks: an extension of metabolic control analysis to non-steady state trajectories. *J Theor Biol* **222,** 23–36 (2003).
10. Stefanini, M. O., Wu, F. T., Mac Gabhann, F. & Popel, A. S. The presence of VEGF receptors on the luminal surface of endothelial cells affects VEGF distribution and VEGF signaling. *Plos Comput Biol* **5,** e1000622 (2009).
11. Hazarika, S. *et al.* Impaired angiogenesis after hindlimb ischemia in type 2 diabetes mellitus: differential regulation of vascular endothelial growth factor receptor 1 and soluble vascular endothelial growth factor receptor 1. *Circ Res* **101,** 948–956 (2007).
12. Hazarika, S. *et al.* MicroRNA-93 controls perfusion recovery after hindlimb ischemia by modulating expression of multiple genes in the cell cycle pathway. *Circulation* **127,** 1818–1828 (2013).
13. Yen, P., Finley, S. D., Engel-Stefanini, M. O. & Popel, A. S. A two-compartment model of VEGF distribution in the mouse. *PloS one* **6,** e27514 (2011).
14. Wu, F. T. *et al.* VEGF and soluble VEGF receptor-1 (sFlt-1) distributions in peripheral arterial disease: an in silico model. *Am J Physiol Heart Circ Physiol* **298,** H2174–2191 (2010).
15. Li, C. & Wang, J. Quantifying the underlying landscape and paths of cancer. *J R Soc Interface* **11,** 20140774 (2014).
16. Weddell, J. C. & Imoukhuede, P. I. Quantitative characterization of cellular membrane-receptor heterogeneity through statistical and computational modeling. *Plos One* **9,** e97271 (2014).
17. Finley, S. D. & Popel, A. S. Predicting the effects of anti-angiogenic agents targeting specific VEGF isoforms. *The AAPS journal* **14,** 500–509 (2012).
18. Woolard, J. *et al.* VEGF165b, an inhibitory vascular endothelial growth factor splice variant: mechanism of action, *in vivo* effect on angiogenesis and endogenous protein expression. *Cancer Res* **64,** 7822–7835 (2004).
19. Cebe Suarez, S. *et al.* A VEGF-A splice variant defective for heparan sulfate and neuropilin-1 binding shows attenuated signaling through VEGFR-2. *Cell Mol Life Sci* **63,** 2067–2077 (2006).
20. McGuigan, M. R. *et al.* Resistance training in patients with peripheral arterial disease: effects on myosin isoforms, fiber type distribution, and capillary supply to skeletal muscle. *The journals of gerontology. Series A, Biological sciences and medical sciences* **56,** B302–310 (2001).
21. Askew, C. D. *et al.* Skeletal muscle phenotype is associated with exercise tolerance in patients with peripheral arterial disease. *Journal of vascular surgery* **41,** 802–807 (2005).
22. McGuigan, M. R. *et al.* Muscle fiber characteristics in patients with peripheral arterial disease. *Medicine and science in sports and exercise* **33,** 2016–2021 (2001).
23. Regensteiner, J. G. *et al.* Chronic changes in skeletal muscle histology and function in peripheral arterial disease. *Circulation* **87,** 413–421 (1993).
24. Finley, S. D., Engel-Stefanini, M. O., Imoukhuede, P. I. & Popel, A. S. Pharmacokinetics and pharmacodynamics of VEGF-neutralizing antibodies. *BMC systems biology* **5,** 193 (2011).
25. Imoukhuede, P. I. & Popel, A. S. Quantitative fluorescent profiling of VEGFRs reveals tumor cell and endothelial cell heterogeneity in breast cancer xenografts. *Cancer medicine* **3,** 225–244 (2014).
26. Mac Gabhann, F. & Popel, A. S. Targeting neuropilin-1 to inhibit VEGF signaling in cancer: Comparison of therapeutic approaches. *Plos Comput Biol* **2,** e180 (2006).
27. Stefanini, M. O., Wu, F. T., Mac Gabhann, F. & Popel, A. S. A compartment model of VEGF distribution in blood, healthy and diseased tissues. *BMC Syst Biol* **2,** 77 (2008).
28. Bhattacharjee, G., Asplin, I. R., Wu, S. M., Gawdi, G. & Pizzo, S. V. The conformation-dependent interaction of alpha 2-macroglobulin with vascular endothelial growth factor. A novel mechanism of alpha 2-macroglobulin/growth factor binding. *J Biol Chem* **275,** 26806–26811 (2000).
29. Fuh, G., Garcia, K. C. & de Vos, A. M. The interaction of neuropilin-1 with vascular endothelial growth factor and its receptor flt-1. *J Biol Chem* **275,** 26690–26695 (2000).
30. Wu, F. T., Stefanini, M. O., Mac Gabhann, F. & Popel, A. S. A compartment model of VEGF distribution in humans in the presence of soluble VEGF receptor-1 acting as a ligand trap. *Plos One* **4,** e5108 (2009).
31. Hudson, N. W., Kehoe, J. M. & Koo, P. H. Mouse alpha-macroglobulin. Structure, function and a molecular model. *Biochem J* **248,** 837–845 (1987).
32. Imber, M. J. & Pizzo, S. V. Clearance and binding of two electrophoretic "fast" forms of human alpha 2-macroglobulin. *J Biol Chem* **256,** 8134–8139 (1981).

Acknowledgements

Author Contributions

L.H.C., V.C.G., B.H.A. and A.S.P. proposed the idea; L.H.C. and G.C. implemented the simulations; V.C.G. and M.H.C. conducted the experiments; L.H.C., V.C.G., S.D.F., B.H.A. and A.S.P. edited the paper. The authors thank Drs. Hojjat Bazzazi and Feilim Mac Gabhann for critical comments and suggestions.

Additional Information

Supplementary information accompanies this paper at http://www.nature.com/srep

Competing financial interests: The authors declare no competing financial interests.

How to cite this article: Chu, L.-H. *et al.* A multiscale computational model predicts distribution of anti-angiogenic isoform VEGF$_{165b}$ in peripheral arterial disease in human and mouse. *Sci. Rep.* **6**, 37030; doi: 10.1038/srep37030 (2016).

Publisher's note: Springer Nature remains neutral with regard to jurisdictional claims in published maps and institutional affiliations.